Delft University of Technology

Uplift and sea level constraints on 3-D upper mantle viscosity in Northern Europe

Blank, B.; Bradley, Sarah L.; van der Wal, W.

Geophysical Journal International

Uplift and sea level constraints on 3-D upper mantle viscosity in Northern Europe

Bas Blank,[1,2] Sarah L. Bradley[3] and Wouter van der Wal [1]

[1]*Faculty of Aerospace Engineering, Delft University of Technology, Kluyverweg 1, 2629 HS, Delft , the Netherlands. E-mail: w.vanderwal@tudelft.nl*
[2]*Institute for Marine and Atmospheric Research Utrecht, Utrecht University, Princetonplein 5, 3584 CC, Utrecht, the Netherlands*
[3]*School of Geography and Planning, University of Sheffield, Winter St, S37ND, Sheffield , UK*

SUMMARY

Northern Europe experiences vertical land motion and sea level changes as a consequence of past changes in ice sheet cover in Fennoscandia and the British Isles. The process, called glacial isostatic adjustment (GIA), is controlled by the subsurface structure. Numerical models of GIA can be compared to observations of uplift or past sea level changes to constrain the subsurface structure, and such models can also be used to correct present-day sea level observations to reveal sea level changes due to climate change. GIA models for northern Europe usually adopt a homogeneous upper mantle viscosity even though seismic studies indicate contrasting elastic lithosphere thickness and upper mantle structure between Northwestern Europe and Eastern Europe. This raises the question whether the effect of lateral variations in structure (3-D viscosity) can be detected in observations of GIA and whether including such variations can improve GIA model predictions. In this study, we compare model output from a finite element GIA model with 3-D viscosity to observations of paleo sea level and current vertical land motion. We use two different methods to derive 3-D viscosities, based on seismic velocity anomalies and upper mantle temperature estimates. We use three different reconstructions of the Eurasian ice sheet, one based on an inversion using a 1-D viscosity model, and two others based on glacial geology and modelling. When we use these two reconstructions, we find that the data are fit better using 3-D viscosity models. Models with two separate 1-D viscosities for Fennoscandia and for the British Isles cannot replicate a 3-D model because a 3-D model redistributes GIA-induced stresses differently from a combination of models with 1-D viscosities. The fit to data across Fennoscandia is improved when, as indicated by seismic models, the upper mantle viscosity is higher than for the rest of Northern Europe. The best fit is obtained with a model with dry olivine rheology, in agreement with other evidence from Fennoscandia.

Key words: Composition and structure of the mantle; Loading of the Earth; Sea level change; Rheology: mantle; Europe; Numerical Modelling.

1 INTRODUCTION

Glacial isostatic adjustment (GIA) is the Earth's response to the formation and decay of large ice masses. It plays a significant part in determining changing sea levels and evolving coastlines. For example, sea level change in northern Europe varies with location primarily due to GIA. The GIA induced vertical land motion (VLM) in the Baltic Sea leads to a sea level fall of about 7–8 mm yr^{-1} (Mäkinen *et al.* 2006; Richter *et al.* 2012), which is about two times higher than the global mean sea level rise (Simon *et al.* 2021). In Scotland, the present-day sea level rise falls with 1.2 mm yr^{-1} (Bradley *et al.* 2023), while the North-western German coast experiences a sea level rise that is 3 mm yr^{-1} above the

global average (Wahl *et al.* 2010). The increased sea level rise in North-western Germany is in large part due to the collapse of the forebulge induced by GIA. To quantify regional sea level change due to recent climate change, it is necessary to correct for the GIA signal. In the Baltic Sea, GIA is the dominant mechanism for sea level change and is measured by global navigation satellite system (GNSS) observations with a high accuracy (±0.12 mm yr^{-1} in the vertical direction) (Kierulf *et al.* 2021). However, in other areas the signal is more complicated, and models are required to calculate the GIA contribution to ongoing sea level change (Simon & Riva 2020), river evolution and past drainage (Peeters *et al.* 2015), or to separate tectonic and GIA deformation (Marotta & Sabadini 2002).
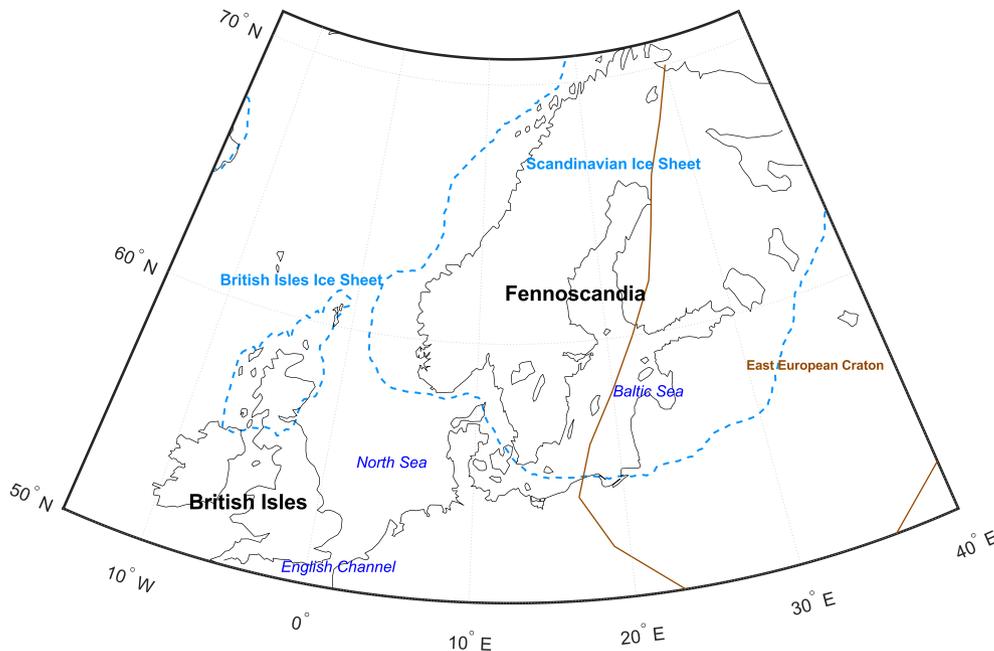
Figure 1. Overview of regions, seas, ice sheets and seismic features in Europe relevant for this study. With the exception of Fig. 2, this projection is the standard projection for all figures shown in this study.

The prediction accuracy of GIA models depends on the ice history and the Earth parameters for rheology. Current models for (parts of) Northern Europe assume the rheology parameters vary only in depth (1-D) (e.g. Steffen & Kaufmann. 2005; Bradley *et al.* 2011; Lambeck et al. 1998). However, seismic studies have shown a significant difference in wave speed between Fennoscandia and Western Europe (Shapiro & Ritzwoller 2002; French *et al.* 2013; Schaeffer & Lebedev 2013; Debayle *et al.* 2016; Fichtner *et al.* 2018; Celli *et al.* 2021). Fennoscandia and the Baltic states have been identified as having an old (>3 Gy) and thick lithosphere called the Baltic shield, which is part of the larger East European Craton (Fig. 1). Beneath the cratonic lithosphere, relatively high seismic velocities indicate low mantle temperature. Therefore, viscosity underneath the Baltic Shield is expected to be up to several orders of magnitude higher than under the rest of Europe (van der Wal *et al.* 2013). Seismic wave speed anomalies can also be observed in the shallow upper mantle of the North Sea stretching out underneath the east and south coasts of Britain (Fichtner *et al.* 2018; Celli *et al.* 2021), though these anomalies are not consistent between all models (French *et al.* 2013; Debayle *et al.* 2016). Based on the changes in properties identified in all seismic models, including 3-D viscosity into GIA models should improve the accuracy of the model predictions. In the following, models with 3-D viscosity are labelled as 3-D models. Models with viscosity that varies in radial direction only are labelled as 1-D models.

Table 1 presents GIA models which adopt 1-D viscosities and are constrained by data from either Fennoscandia or the British Isles. The studies by Fjeldskaar et al. (1994; 1997) study the effect of the asthenosphere and focus on a regional data set and are not included in the overview. It can be seen that upper mantle viscosities range from 4–7 × 10^20 Pa·s for Fennoscandia and 3–7 × 10^20 Pa·s for the British Isles. Thus, GIA inferences do not support the large contrast in Earth properties found in seismic data. Contrary to this, a comparison of GIA models with data from the GRACE (Gravity Recovery And Climate Experiment) satellite mission data for Fennoscandia and for the neighbouring Barents Sea region (not studied in this

paper) find an upper mantle viscosity in Fennoscandia of a factor of two higher compared to the Barents Sea, which agrees with viscosity ratios between the two regions derived from seismic models (Rovira-Navarro *et al.* 2020). A more direct indication is given in Steffen *et al.* (2014), who use multiple 1-D models to fit the data in small regions underneath Europe. They find that for areas under the Baltic Sea the best fit is obtained using high viscosity (20 × 10^20 Pa·s) which is an order of magnitude higher than what they find for the Oslo area in the western part of Fennoscandia. The only aspect in which regional GIA models of the British Isles and Fennoscandia differ is the elastic lithosphere thickness. Bradley *et al.* (2011) and Steffen & Kaufmann (2005) find a best-fitting elastic lithosphere of 70 km for the British Isles, which is close to the elastic lithosphere thickness of 75 km found for all of Europe (Lambeck *et al.* 1998). The elastic lithosphere found for Fennoscandia is considerably larger with a thickness ranging from 80 km (Klemann & Wolf 2005; Steffen & Kaufmann 2005) to 160 km (Kierulf *et al.* 2014 Vestøl *et al.* 2019) with most studies finding a lithosphere thickness larger than 100 km.

Two studies (van der Wal *et al.* 2013; Kierulf *et al.* 2014) compared results for spherical finite element method (FEM) 3-D GIA models against results with 1-D models. Van der Wal *et al.* (2013) using ICE-5G and a custom-made ice model concluded that some 3-D models outperformed the 1-D models in terms of fit to relative sea level (RSL) and VLM data. Kierulf *et al.* (2014) found the 1-D model results in better fit to VLM data than the 3-D model, apart from Northern Norway. Here it must be noted that the ice histories used in the latter study are built by fitting a 1-D GIA model to the data and will therefore have an inherent bias towards a specific 1-D model. Data inversion GIA models also show the largest discrepancies with 1-D models such as ICE-6G in Fennoscandia (Simon & Riva 2020), which could be explained by 3-D viscosities that are not in the 1-D model. Both van der Wal *et al.* (2013) and Kierulf *et al.* (2014) focused only on the Scandinavian ice sheet (SIS) and used fewer data than are currently available. Furthermore, both only considered a single ice sheet history or only ice histories

Table 1. An overview of 1-D GIA model findings for the Earth structure in Europe according to different studies.

	British isles		Fennoscandia	
	Lithosphere thickness [km]	Upper mantle viscosity [10^{20} Pa·s]	Lithosphere thickness [km]	Upper mantle viscosity [10^{20} Pa·s]
(Lambeck et al., 1998)	∼75	3.6	∼75	3.6
(Steffen & Kaufmann 2005)	60–70	4	∼120	4
(Lambeck 1993; Lambeck *et al.* 1996)	70	4–5	–	–
(Kaufmann & Lambeck 2000)	70–120	7		
Bradley *et al.* (2011)	71	4–6		
(Kuchar *et al.* 2012)	71	3		
(Wieczerkowski *et al.* 1999)	–	–	70–120	5
(Fleming *et al.* 2002)	–	–	110	5
(Klemann & Wolf 2005)			80	5
(Milne *et al.* 2001, 2004)	–	–	90–170	5–10
(Steffen *et al.* 2010)	–	–	160	4
(Lidberg *et al.* 2010)	–	–	120	5
(Zhao *et al.* 2012)	–	–	93–110	5
(Kierulf *et al.* 2014)	–	–	140	7
(Vestøl *et al.* 2019)	–	–	160	7

strongly based on an assumed 1-D rheology and the resolution for both models (2° × 2°) is too coarse to model details in coastlines reliably.

Li & Wu (2019), using ICE-6G_C, found a better fit of observed data for both North America and Fennoscandia when including a laterally varying elastic lithosphere but concluded the fit deteriorated when also including a laterally varying upper mantle. 3-D GIA models have been used in other regions with marked lateral viscosity variations. Results show that using 3-D viscosity can improve the fit to observed data, in for example, Antarctica (Powell *et al.* 2022) and North America (Kuchar *et al.* 2019a), compared to 1-D models, but other studies were unable to find unambiguous improvements for 3-D models in North America (Yousefi *et al.* 2021) and Antarctica (Blank *et al.* 2021). Possible reasons why the fit for 3-D models might not always improve even though lateral viscosity variations are very likely to exist are the limited parameter studies of 3-D models because of the large computation time, and the input ice models that are created based on 1-D Earth models and uncertainties in 3-D viscosities (Steffen *et al.* 2006).

In this study, we address the discrepancy between seismic studies that show lateral variations in the mantle underneath Europe and the relatively homogeneous upper mantle viscosity found with regional 1-D GIA models. We do so by comparing the fit of 3-D and 1-D models with measured RSL and VLM data and by using recent ice histories that have been constructed using additional geological constraints, which reduces the inherent bias towards 1-D Earth model. Because of the large computation time of the 3-D models, we limit ourselves to lateral variations between 70 and 400 km for which we have a global thermomechanical model (WINTERC-G; Fullea *et al.* 2021) and for which the olivine flow laws used for part of the 3-D models are valid.

Our main objective is to find out to what extent GIA models with 3-D rheology in north–western Europe improve the fit to RSL and VLM data compared to conventional 1-D rheology. The research questions are (i) do 1-D or 3-D viscosity models fit the data in northern Europe better and why? (ii) is the data sensitive to 3-D structure even when averaged viscosities are close to those of 1-D viscosity models? (iii) does the data in the British Isles and Fennoscandia favour a 3-D model which results in a large viscosity contrast between the regions? Answering these questions will also provide improved knowledge on the Earth's structure underneath

Europe. Secondly, an improved GIA model will improve estimates of climate-induced sea level changes, tectonic motion, and landscape evolution studies, by providing a better GIA correction for tide gauge data, GNSS or RSL data.

2 METHOD

This section discusses the GIA model (Section 2.1) and its inputs which consist of different 3-D viscosities (Section 2.2) and three different ice sheet reconstructions (Section 2.3). We produced RSL and VLM predictions for each of the three ice sheet reconstructions combined with (a subset of) 21 3-D viscosity profiles and several 1-D viscosity profiles, which results in a total of 42 model combinations, and analysed the fit to the RSL and VLM data that are discussed in Section 3.

2.1 GIA model

The 3-D GIA model used is the spherical FEM from Blank *et al.* (2021). It is based on the formulation of Wu (2004) which uses the commercial software package ABAQUS in combination with stress transformation and iteration to create a self-gravitating GIA model. Self-consistent sea levels with migrating shorelines (e.g. Kendall *et al.* 2005) as well as geocentre motion (e.g. Tanaka *et al.* 2009) are also included in the model. In our implementation, the grid resolution in the region of interest is around 40 km in a spherical cap centred on the Danish Islands (58°N 11°E) with a radius of 17 spherical degrees (see Supplementary Section S.2). The grid size for the sea level equation is higher than the FEM (∼25 km) to be able to include an increased resolution to represent the complex coastline. The present-day topography is interpolated to this grid from ETOPO1 (Amante & Eakins 2009).

The layering is the same as in Blank *et al.* (2021) with a minimum elastic lithospheric layer of 70 km based on the minimal elastic thickness found by GIA studies underneath the British Isles (Bradley *et al.* 2011). The upper mantle is divided into the shallow upper mantle (70–180 km), deep upper mantle (180–400 km) and transition zone (400–670 km), as in Barletta *et al.* (2018) and Blank *et al.* (2021). This layering allows us to focus more on the viscosity differences in the first 180 km of the upper mantle. The 3-D viscosities are applied in the shallow and deep upper mantle layers, as the

flow laws and seismic wave anomaly conversion methods we use to determine viscosity are not applicable below 400 km. Additionally, the transition zone has less lateral variation in seismic velocities in the study region (Schaeffer & Lebedev 2013). 3-D viscosity models in the upper mantle are discussed in the next section. Viscosity in the lower mantle is set to 3×10^{21} Pa·s close to the VM2 profile (Peltier 2004) also used in Kierulf *et al.* (2014). Changing transition zone viscosity affects VLM and RSL and thus possibly the best fit, as will be investigated in Supplementary Section S.8. Lateral variations in the transition zone affect horizontal velocities but have a relatively small effect on uplift (Steffen *et al.* 2006).

2.2 3-D viscosity

We use two different input upper mantle models to derive the input 3-D viscosities: upper mantle temperature model WINTERC-G (Fullea *et al.* 2021) and seismic model SMEAN2 (Jackson *et al.* 2017). WINTERC-G is an upper mantle model obtained from an integrated geophysical–petrological approach, in which seismic data, gravity data and thermobarometric data are inverted. The model assumes isostasy and the fit to the data sets is obtained by changing the mantle's mineralogical composition, creating a temperature distribution for the upper 400 km of the Earth. SMEAN2 is an average of three tomography models, SAVANI, GyPSuM and S40RTS. As SMEAN2 is an averaged model, it is by nature a smoother model with less pronounced features. However, it is more robust than those individual seismic models (Jackson *et al.* 2017). To convert the seismic wave anomalies into temperatures for SMEAN2 the following relationship is used:

$$T = T_{\text{ref}} \left[1 + \frac{\partial T}{\partial v_s} \frac{\delta v_s}{v_s} \right] \tag{1}$$

Here T_{ref} is the global reference temperature from Turcotte & Schubert (2002), $\frac{\partial T}{\partial v_s}$ the temperature-wave speed derivative (Karato 2008) and $\frac{\delta v_s}{v_s}$ the seismic wave speed anomaly. All quantities are depth dependent.

The first method we use to obtain viscosity is a scaling of seismic velocity anomalies (Ivins & Sammis 1995) used here in the form of Wu *et al.* (2013), which can only be applied to SMEAN2 for our study:

$$\log_{10}\eta = -0.4343\beta \frac{\partial T}{\partial \ln v_s} \frac{\delta v_s}{v_s} \frac{E + PV}{RT^2} + \log_{10}\bar{\eta} . \tag{2}$$

Here E is the activation energy, V is the activation volume, R is the universal gas constant, T is the temperature as computed in eq. (1) and P represents the pressure, which is computed based on the hydrostatic pressure that follows from the undisturbed model. Furthermore, $\bar{\eta}$ represents the 1-D background viscosity and β a scaling factor that is equal to 1 when all seismic velocity anomalies are caused by thermal anomalies, and 0 when seismic velocity anomalies are only caused by compositional changes that do not manifest as viscosity anomaly. The background viscosity is taken from the reference viscosity model VM5a (Peltier *et al.* 2015) and is set to 5×10^{20} Pa·s for the upper mantle.

In the second method, the 3-D rheologic parameters are derived from the temperature estimates of SMEAN2 and WINTERC-G using the flow laws for diffusion creep and dislocation creep in olivine (Hirth & Kohlstedt 2004). The creep mechanisms are assumed to act simultaneously which results in a so-called composite rheology (e.g. van der Wal *et al.* 2010). The change in uniaxial equivalent strain increment $\Delta\tilde{\epsilon}$ is related to the von Mises equivalent stress $\tilde{q}$

and time increment Δt with the creep coefficient B according to:

$$\Delta\tilde{\epsilon} = B\tilde{q}^n \Delta t \tag{3}$$

with the stress exponent n equal to 3.5 (Hirth & Kohlstedt 2004). The strain is linearly dependent on stress for $n = 1$; the rheology is nonlinear for $n > 1$. The individual contribution of either diffusion B_{diff} and dislocation creep B_{disl} is determined by (Hirth & Kohlstedt 2004):

$$B = Ad^{-p} f_{H_2o}^r e^{-\frac{E+PV}{RT}} . \tag{4}$$

For dislocation and diffusion creep, different values for the parameters A, p and r are obtained experimentally (Hirth & Kohlstedt 2004).

The effective viscosity η_{eff} is determined by the combined contributions from the diffusion B_{diff} and dislocation creep B_{disl} in an element in accordance with Blank *et al.* (2021) based on the derivation from van der Wal *et al.* (2013):

$$\eta_{\text{eff}} = \frac{1}{3B_{\text{diff}} + 3B_{\text{disl}}\tilde{q}^{n-1}}. \tag{5}$$

It is important to note that the effective viscosity becomes stress dependent for rheologies where dislocation creep plays an important role, which is the case for most wet rheologies (Hirth & Kohlstedt 2004). For the nonlinear rheology, we mostly used models with a homogeneous grain size and water content but we also created models using SMEAN2 where we increased the grain size for the mantle below the cratonic lithosphere to reflect possible grain growth over time. The threshold to identify a region as cratonic is at a positive seismic wave speed anomaly of 2 per cent. For SMEAN2 the temperature from eq. (1) is inserted in eq. (4), calculating the creep parameter, which in turn can be used in eq. (5) to compute the effective viscosity. While changing both grain size and water content can alter viscosity values, it is important to note that changing the water content has a larger effect on the nonlinear behaviour than grain size has. Using this approach we developed 42 earth models (see Supplementary Section S.6), varying β between 0.25 and 0.75, grain size between 4 and 10 mm and water content between 0 and 1000 ppm.

Fig. 2 shows the 3-D viscosity models which produced the optimum fit to both the RSL and VLM data (with ICE-6G for WINTERC-G 7 mm dry, and with BRITICE for SMEAN2 Hybrid 4/8.5 mm). Both models show high-viscosity anomalies in Finland and North-Eastern Europe. The models based on SMEAN2 have a relatively homogeneous viscosity, slightly higher than the background viscosity, extending from western Norway across the North Sea and the British Isles. For the WINTERC-G based Earth models there is a high-viscosity feature from the coast of Norway, extending across the North Sea down to south of the English Channel at 110 km (Fig. 2a), which is absent in deeper layers (Figs 2b and c).

To compare 3-D models with 1-D viscosity models, an average viscosity is calculated from the 3-D viscosity models in three steps. First, we select which elements contribute significantly to relaxation, which we define as being strained by more than 20 per cent of the maximum element strain at that depth, similar to Blank *et al.* (2021) with the difference that elements are selected based on strain instead of stress. This change is made as highly viscous elements from the Baltic Shield would accumulate high stresses without contributing directly to VLM. Secondly, we filter out any element that has an effective viscosity upwards of 10^{23} Pa·s as these elements are deemed to behave elastically on the timescale considered. The average thickness of the layer of elements above 10^{23} Pa·s is considered the effective elastic lithosphere thickness. Finally, from the
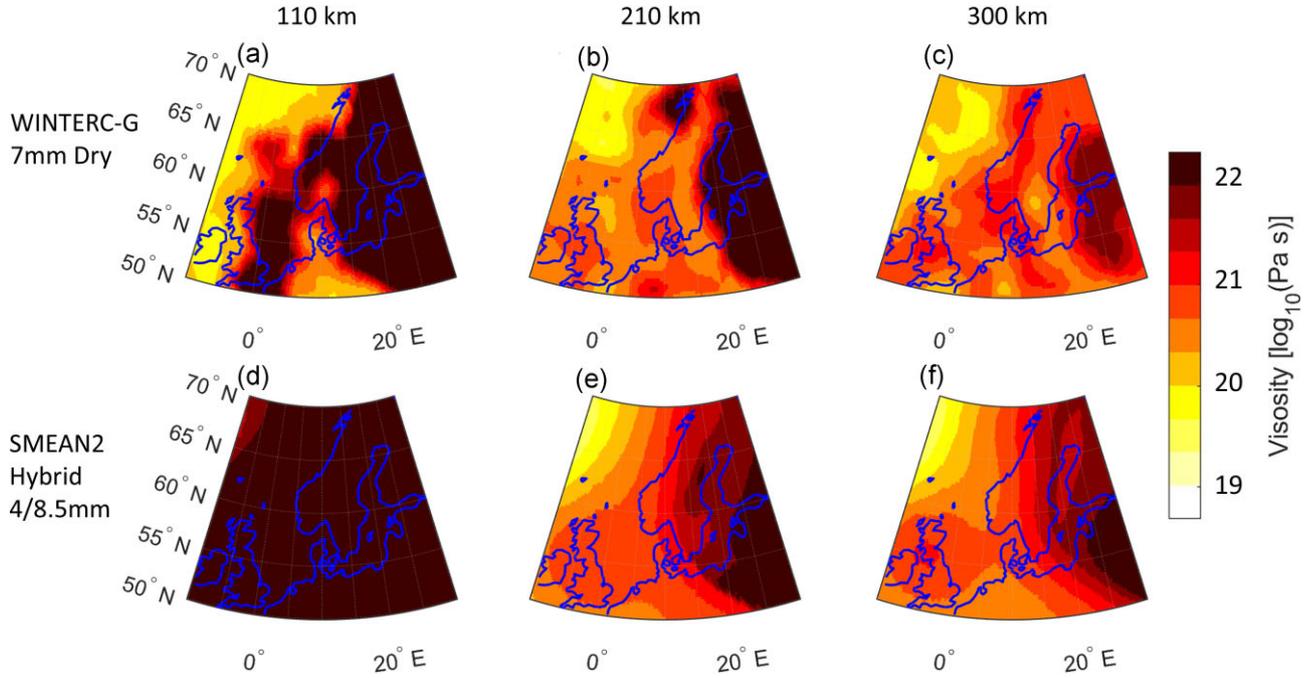
Figure 2. Viscosity at three depths, 110 km (a and d), 210 km (b and e) and 300 km (c and f) for the WINTERC-G model with 7 mm grain size and dry conditions (a, b and c) and the SMEAN2 model with 8.5 mm grain size in cratonic regions and 4 mm elsewhere (d, e and f). All values are $\log_{10}$ of the viscosity in Pa·s.

remaining selection of contributing viscous elements we take the average of the $\log_{10}$ of the viscosity.

2.3 Ice sheet reconstructions

For this study three different ice sheet reconstructions for Europe were used, which have varying dependence on a 1-D Earth model. The first is ICE-6G_C (From here on, ICE-6G), which has been developed to match far-field and near-field RSL and VLM data using the VM5a viscosity model (Peltier *et al.* 2015). VM5a has a 60 km elastic lithosphere followed by a 40 km layer with 10^{23} Pa·s, the rest of the upper mantle (100–670 km) has a viscosity of 5×10^{20} Pa·s. The data used partially overlap with the RSL and VLM data used in this paper. This ice history is inherently biased towards the VM5a viscosity model. The previous iteration of ICE-6G, ICE-5G, shows relatively large misfits for areas in Fennoscandia which a 3-D model could possibly resolve (Kierulf *et al.* 2014). The second is the ice sheet created within the BRITICE-CHRONO project, which will be referred to as the BRITICE model. The focus of the BRITICE model has been on reconstructing the ice sheets over the British Isles, North Sea and Fennoscandia using glacial geomorphological data (Hughes *et al.* 2016; Clark *et al.* 2018) and geochronological data as constraint for the ice sheet extent at different time steps. The ice sheet reconstruction was developed independent of RSL data. The SIS was constrained to fit the DATED-1 reconstruction (Hughes *et al.* 2016). To create the ice thickness for all ice sheets ICESHEET 1.0 (Gowan *et al.* 2016) was used. ICESHEET 1.0 is a plastic ice model underlain by a 1-D Earth model with an upper mantle viscosity of 4×10^{20} Pa·s. The third ice reconstruction is from Patton *et al.* (2017) and will be referred to as the P17 ice model. It uses a thermomechanical model to model the ice sheet build up (Patton *et al.* 2016) and deglaciation (Patton *et al.* 2017) of the European ice sheet. Observed flow channels and marginal

moraines are used to calibrate the flow patterns of the model. Finally, to calibrate local ice thickness a 1-D Earth model with an upper mantle viscosity of 3×10^{20} Pa·s was used to model GIA that upon iteration best fits the RSL data in combination with the ice sheet input. The ice thickness of all ice histories at selected epochs is shown in Supplementary Section S.4. Outside Europe, the ice history of ICE-6G was used for the ice thickness in all models.

Because the P17 and BRITICE models are both largely constrained on geological data and ice evolution models, they have a weaker bias to a 1-D Earth than ICE-6G has. There is some overlap in RSL data and geomorphological data, but the differences in methodology and data used are large enough that the P17 and BRITICE ice histories are distinctly different (see Supplementary Section S.4). While there are more results generated with ICE-6G for this study, we choose not to repeat Earth models for the P17 models that performed very poorly to save on computation resources. At the same time the results for the low scoring Earth models were also not discarded as knowing which models are performing poorly can reveal information about the mantle by the process of elimination.

2.4 RSL and VLM data

For the RSL data we combined RSL data sets from across Europe (García-Artola *et al.* 2018; Shennan *et al.* 2018; Hijma & Cohen 2019; Rosentau *et al.* 2021; Creel *et al.* 2022). This results in a combined data set of 4090 sea level index points (SLIP) and a larger spatial coverage than in previous studies (van der Wal *et al.* 2013; Kierulf *et al.* 2014). To avoid spatial bias from locations with more data we weighted each (SLIP) data point based on its proximity to other SLIP's (including itself) in terms of location (<200 km) and time (<1 ka) (see also Fig. 3a):

$$W_{RSLi} = \frac{1}{n_{SLIP(<200km\ \&<1ka)}} \qquad (6)$$
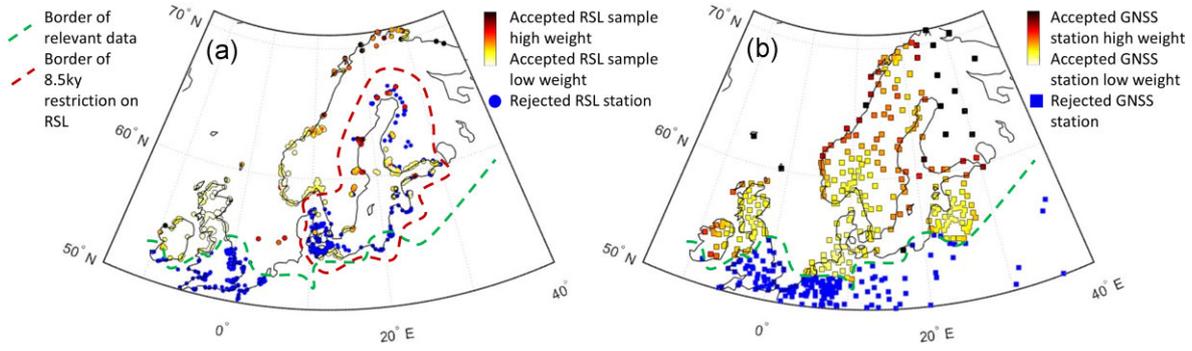
Figure 3. Locations of RSL data (a) and VLM data (b) used in this study. Both the accepted RSL data (a) and VLM data (b) are shown in colours denoting the weights according to the colour scale while rejected data are shown in blue.

A large part of the data from Rosentau *et al.* (2021) for the Baltic Sea region is dated to time periods where the Baltic Sea was either a lake or in a transitional state. As we do not model lake effects, we removed the data when the Baltic Sea was not a sea, which is considered to be for ages before 8.5 ky B.P. (Rosentau *et al.* 2021).

We filtered the data to retain only RSL and VLM data which have a significant GIA signal caused by the Eurasian ice sheet, as including other data would bias results towards models with little GIA response. We define these as data lying in any region in Europe where the variation between all models is at least 20 per cent of the maximal variation between models at any point in time (as indicated in Fig. 3a by a blue square for the GNSS station or circle for the SLIP's).

For the RSL data, we compute the misfit as follows:

$$\text{Misfit}_{\text{RSL}} = \frac{\sum_{i=1}^{n_{\text{RSL}}} W_{\text{RSL}_i} \sqrt{\left(\frac{\text{RSL}_{o,i} - \text{RSL}_{m,i}}{\sigma_{\text{RSL}i}}\right)^2}}{n_{\text{RSL}}}, \quad (7)$$

where $\text{RSL}_{o,i}$ is the observed RSL at location i, $\text{RSL}_{m,i}$ the modelled RSL at the same location i. The difference between both is normalized by the standard deviation attributed to the observed height, $\sigma_{\text{RSL}i}$. Furthermore, n_{RSL} is the total number of data points. The absolute distance in RSL height between model and data point is used instead of distance squared because otherwise the misfit would be controlled by a few points with very large differences between model and observations, as the measurement error is a relatively small part of the total RSL variation between models, which can be influenced by within-estuary processes or short-term oscillations in sea level (Shennan *et al.* 2018). We randomly sampled 2/3 of the data points a 1000 times in order obtain a distribution for every model. T-tests can be performed using these distributions to test whether models differ significantly from each other. For more consideration on this choice, we refer to Supplementary Section S.10.

For the data for the VLM we have used data from the Tide Gauge working group (TIGA), the BIFROST (Baseline Inference for Fennoscandian Rebound Observations, Sea level and Tectonics) network (Kierulf *et al.* 2021) and Schumacher *et al.* (2018), which use the ITRF2008 reference frame. The ITRF2008 reference frame is defined such that there is no translation or translation rate with respect to the mean centre of mass over a certain time frame (Altamimi *et al.* 2011). This can deviate from the centre of mass of the Earth that is taken as reference in our modelling. We assume that this error is small and of such a large wavelength that it will not cause differences in misfit between models. The GNSS data is corrected for elastic deformation due to e.g. atmospheric loading, non-tidal ocean loading, ice mass change, (Schumacher *et al.* 2018;

Kierulf *et al.* 2021) and any overlapping data between sets has been removed.

The VLM data is weighted with the inverse of the density of GNSS observations in a 200 km radius around GNSS station i, creating weight W_{VLMi} to avoid a bias for more densely sampled regions (see also Fig. 3b). The misfit is defined as:

$$\text{Misfit}_{\text{VLM}} = \frac{\sum_{i=1}^{n_{\text{gps}}} W_{\text{VLMi}} \sqrt{\left(\frac{u_{o,i} - u_{m,i}}{\sigma_{ui}}\right)^2}}{n_{\text{gnss}}}. \quad (8)$$

Here u_i and u_m are the measured uplift rate at station location i, and the corresponding modelled uplift rate, respectively. Before adding the misfit of both the RSL and VLM data we normalize the misfit with the value from the model with the median misfit to avoid one data set dominating the misfit:

$$\text{Misfit}_{\text{total}} = \frac{\text{Misfit}_{\text{RSL}}}{\text{medMisfit}_{\text{RSL}}} + \frac{\text{Misfit}_{\text{VLM}}}{\text{medMisfit}_{\text{VLM}}}. \quad (9)$$

3 RESULTS

To assess the importance of the 3-D viscosities profiles, seven runs are performed with 1-D viscosity profiles only. Each of the three ice histories is combined with the VM5a viscosity profile, to be able to compare the effect of different ice histories. Furthermore, ICE-6G and BRITICE are combined with lower (3×10^{20} Pa·s) and higher (5×10^{21} Pa·s) upper mantle viscosity, to investigate the range of sea levels 1-D viscosity models can provide. Of the 34 3-D model runs, 16 are based on SMEAN2 and 18 are based on WINTERC-G. We present model comparisons to the RSL data, to VLM data and to a combination of both data sets to investigate if 3-D viscosity can improve the combined fit. Finally, we evaluate if the average upper mantle viscosities found in 1-D studies for the Fennoscandian and British Isles regions agree with the local viscosity of the best fitting 3-D models.

3.1 Model misfits

We tested the robustness of the assumptions, such as the selected data and sensitivity range for the weights, necessary for eqs (6) and (9) that are used to compute the combined misfit and found that changing them for reasonable alternative assumptions only has a minimal effect on the ranking of the models (see Supplementary Section S.5). The best performing model when just considering the RSL data is a 1-D model with VM5a viscosity profile and a version of VM5a with a lower viscosity in the upper mantle ($\eta = 3 \times 10^{21}$
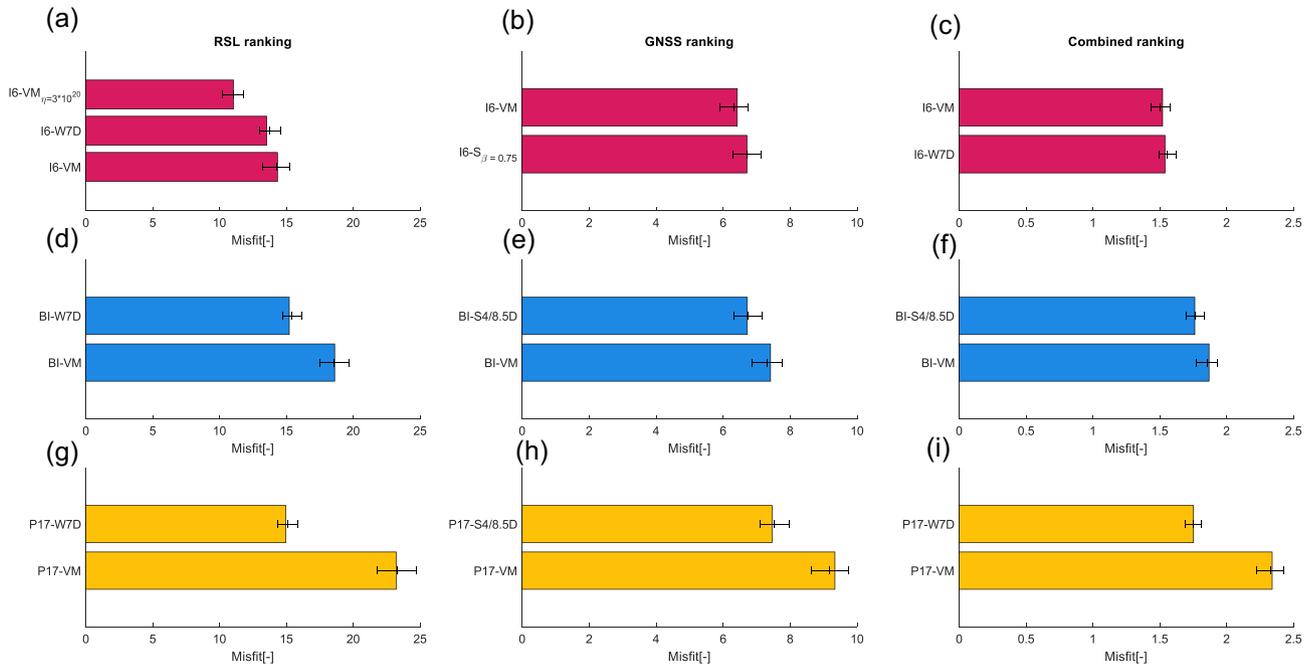
Figure 4. Misfit of the best performing 1-D and 3-D models compared to one another. (a–c) Use the ICE-6G ice history, (d–f) use the BRITICE ice history and (g–i) use the P17 ice history. The first column (a, d, g) shows the misfit compared to the RSL data, the second column (b, d, e) the misfit compared to the GNSS data and the third column (c, f, i) the combined misfit. In panel (a) both I6-VM_$\eta = 3 \times 10^{20}$ and I6-VM are shown, as I6-VM_$\eta = 3 \times 10^{20}$ is technically the best 1-D model compared to RSL data but is disqualified based on the VLM. The error bars are determined by bootstrapping the data and display the median misfit and 95 per cent ranges (see Supplementary Section S.10).

Pa·s), henceforth I6-VM_$\eta = 3$ (see Fig. 4a). It is not surprising that the combination of ICE-6G with its standard Earth model VM5a, henceforth I6-VM, and I6-VM_$\eta = 3$ are performing well as ICE-6G has been developed based on VM5a to fit the majority of the data used here (Peltier *et al.* 2015). Although I6-VM_$\eta = 3$ can fit the data well, it can be rejected as it does not fit higher uplift rates (11 mm yr^{-1}) in central Fennoscandia, predicting a maximum uplift of 6.5 mm yr^{-1} (see Supplementary Section S.7). The second-best model is the 3-D model using ice history ICE-6G and the Earth model WINTERC-G with a uniform grain size of 7 mm (I6-W7D). Also, when comparing to the GNSS data the best performing model is I6-VM, outperforming the best ICE-6G based 3-D model (see Fig. 4b) when the misfit is combined, we unsurprisingly see that the best performing model is I6-VM (Fig. 4c and Table 1). However, 3-D model I6-W7D was able to match the 1-D model results in terms of misfit using the same ice history.

For the ice histories that were not created by fitting the ice model to the RSL data for a 1-D Earth model (BRITICE or P17) 3-D models provide an improvement. When comparing to the GNSS data, we observe that for the ice models that were not specifically fit to local data with a 1-D model there is a significant improvement with 3-D models. As a consequence, for the combined misfits the 3-D models actually improve the fit to the data compared to 1-D models.

3.1 RSL data examination

In order to better understand the results shown in Table 1 and Fig. 2 we look at the RSL data for the best performing 1-D and 3-D models. Fig. 5 shows a map of predicted RSL for the best performing 3-D model (I6-W7D) at 7 ky B.P., and the difference between I6-W7D

and the reference model (I6-VM), in terms of RSL and in terms of misfit. It is worthwhile to know if the effect of 3-D viscosity can be distinguished from that of the reference 1-D model viscosity, which is also the background viscosity for some of the 3-D models. The RSL map in Fig. 5(a) has a different spatial pattern than the difference in Fig. 5(d), unlike the difference between 1-D models in Fig. 5(c). This suggests that the 3-D viscosity could affect the results in a way that cannot be reproduced by another 1-D model, which means that, given there is an ample amount of data from the areas in Fig. 5(d) where the difference is the largest, the 3-D model can be expected to improve fit significantly.

To see where the best performing 3-D model outperforms the reference 1-D model and the best 1-D model we plot misfit difference for each location in Fig. 5(b) and selected modelled sea level curves in Figs 5(e) to (g). The observed RSL in central Fennoscandia (around the Eastern Baltic Sea) is lower than the 1-D models predict but is captured by the model I6-W7D in the entire area. The largest differences between models are at times older than 8.5 ky B.P. but models for that period cannot be compared to data due to the Baltic Lake phases. In the British Isles I6-W7D agrees better with more southern RSL sites, while the 1-D models fit the Northern sites better. In Northern Wales (Fig. 5e), both 1-D models show a rise in RSL from −12 ky to a highstand at −6 ky. After −6 ky, the local uplift speed outpaces the rise in global sea level, thus resulting in a net decline of the RSL. I6-W7D has a longer local relaxation time (as can be inferred from the high viscosity in Fig. 2) and thus the uplift is slower. As a result, the RSL never experiences the highstand. This matches the local RSL data better than the results of both 1-D models with the highstand. This is also remarked in Roberts *et al.* (2011) and Rushby *et al.* (2019), who exclude GIA solutions with highstands in North Wales during the Holocene. In Samsø (Fig. 5f) in the Danish Strait, the apparent highstand in the data over
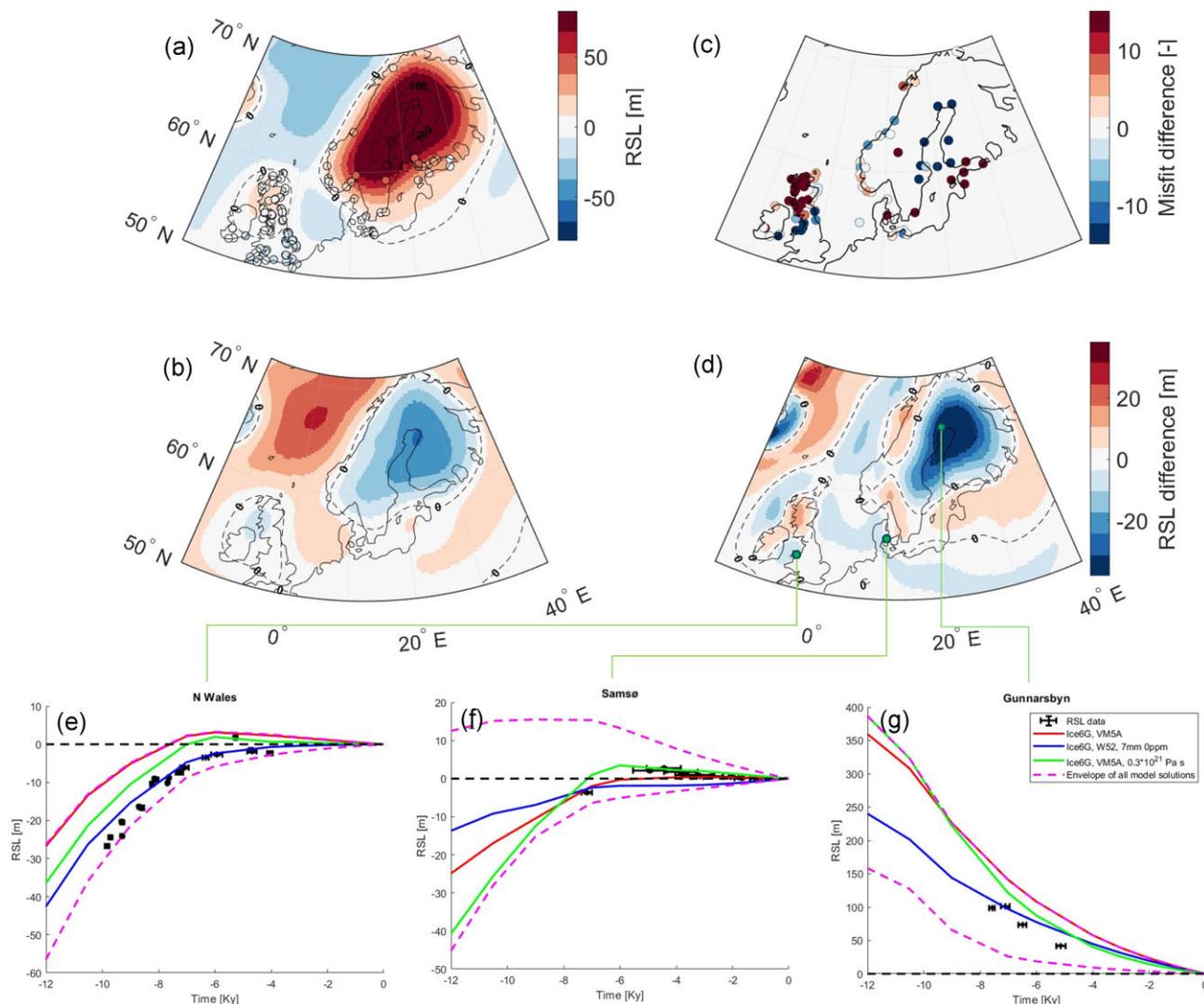
Figure 5. (a) RSL at 7 ky for the best performing 3-D model (ICE-6G with WINTERC-G dry, 7 mm grain size). (b) The improvement of 3-D RSL fit with respect to the reference 1-D RSL fit. Blue sites indicate the 3-D model fits better and red sites indicate the 1-D model fits better. (c) The difference between the best performing 1-D model and the reference 1-D model. (d) The difference between the best performing 3-D model and the reference 1-D model. Locations for the RSL evolution over time at individual sites, North Wales (e), Samsø (f), and Gunnarsbyn (g). For all individual sites (e–g) the RSL over time for the 1-D model is shown in red and for the 3-D model in blue and the overall best model is shown in green. The magenta dotted lines indicate maximal and minimal values found among all models with the same ice history at every time step for those locations.

the last 5 ky in combination with a negative RSL value before this point in time is only possible with substantial initial deflection at LGM (Last Glacial Maximum) and rapid uplift during deglaciation. I6-W7D gives a less negative RSL than both 1-D models initially, with a slower increase over time and hence a poorer fit. In central Fennoscandia, near Gunnarsbyn (Fig. 5g), I6-W7D also produces a lower predicted RSL than the 1-D model, fitting the observed data better.

have a spatial pattern that is likely related to the underlying viscosity as lower uplift for the 3-D model in northern Finland and Sweden occurs where the local viscosity is higher (see Fig. 2). BI-S4/8.5D predicts too low uplift rates in central and eastern Sweden but does well for other areas in Fennoscandia. In Finland and around the Norwegian–Swedish border there is a marked improvement compared to the 1-D model which predicts too high uplift rates.

3.2 VLM data examination

To understand if 3-D models improve the fit to GNSS data compared to 1-D models, Fig. 6 shows the absolute uplift of the best 3-D model that is not based on ICE-6G, BI-S4/8.5D in Fig. 6(a), and the difference in uplift rate between BI-S4/8.5D and the reference 1-D model (BRITICE with VM5a, BI-VM) in Fig. 6(d). The differences

3.3 Combined data regional examination

To see if there are regions where the results are improved using a 3-D viscosity regardless of the exact Earth and ice models used, we compare a 3-D model with a 1-D model for the same ice model. Fig. 7(a) shows the difference between the fit of the best 3-D model, I6-W7D, with that of the reference 1-D model. Fig. 7(b) shows
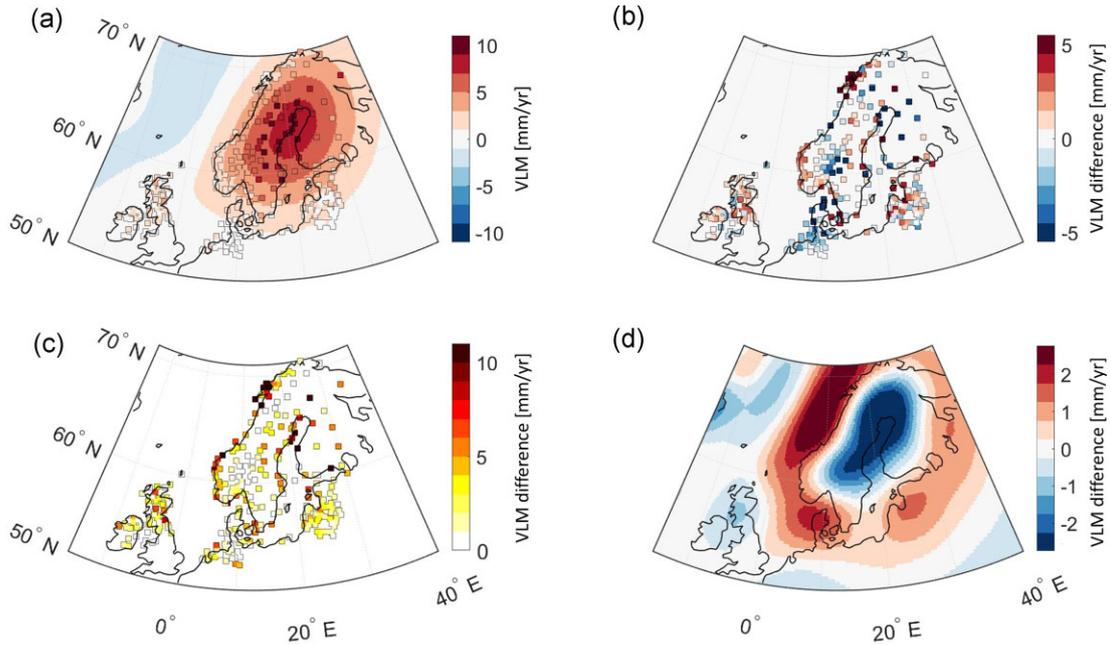
Figure 6. (a) The VLM for the best fitting 3-D model (BRITICE with SMEAN2 model with global 4 mm grain size and cratonic 8.5 mm grain size) with uplift data of GNSS stations as squares overlain. (b) The VLM of the 3-D model minus the VLM of the 1-D reference model at the GNSS stations. Blue indicates improvement for the 3-D model while red indicates improvement for the 1-D model. (c) The absolute difference between observed uplift data and the 3-D model predictions from (a). (d) The best-fitting 3-D model minus the 1-D reference model (BRITICE with VM5a).
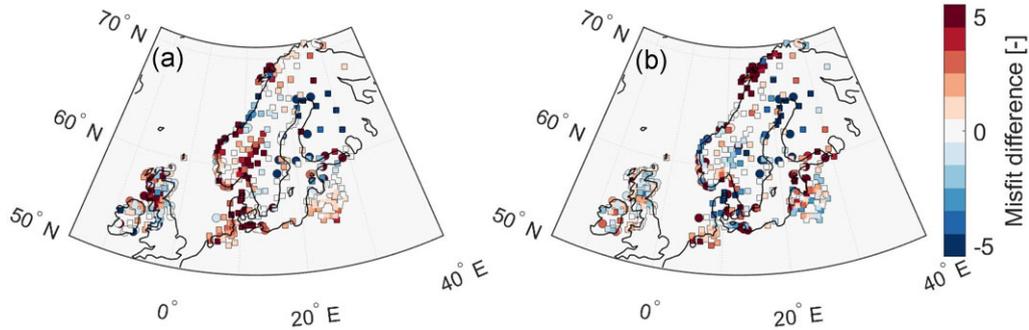
Figure 7. Misfit difference between models. (a) The misfit for ICE-6G with WINTERC-G 7 mm grain size and dry conditions minus the misfit of the reference 1-D model (ICE-6G with VM5a). (b) The misfit for BRITICE with SMEAN2 and $\beta = 0.75$ minus the misfit of BRITICE with VM5a. Red symbols are sites where the 1-D model performs better and blue symbols where the 3-D model performs better.

the difference between the fit of the best-fitting 3-D model, BI-S_$\beta = 0.75$, which has a different ice history, Earth model, and rheology (the BRITICE ice model and scaled rheology based on SMEAN2) with the misfit of BRITICE with VM5a. The area that shows an improvement in fit for both 3-D models is Finland and the Northern Baltic Sea. This area is in the centre of the Scandinavian ice sheet and is underlain by the East European craton. It shows that including a 3-D viscosity structure there helps to reproduce a locally lower uplift because the relaxation is reduced by the higher viscosity and deflection shifts westwards because of lateral viscosity variations (Supplementary Section S.1). Areas that perform poorly in almost all 3-D models are the southwestern Norwegian coast and the Danish Strait. The RSL data suggests that these areas have faster relaxation than produced by most of the 3-D models.

Finally, we want to establish if the British Isles and Fennoscandia favour different 3-D models and therefore we calculated the

misfit for the British Isles and Fennoscandia separately in Table 2. Although some models perform well for both regions, models with low viscosity or wet rheologies perform well for the British Isles but poorly in Fennoscandia. In Fennoscandia, models with higher viscosity, high-lithospheric thickness or both do well.

The median best-fitting models for the British Isles are 0.53×10^{21} Pa·s for the shallow upper mantle and 0.50×10^{21} Pa·s for the deep upper mantle. These viscosities correspond with previous viscosity findings of $0.4 - 0.6 \times 10^{21}$ Pa·s found in 1-D GIA studies for the region (Simms *et al.* 2022; Bradley *et al.* 2023). For Fennoscandia the median of the best-fitting models is 4.9×10^{21} Pa·s for the shallow upper mantle and 1.3×10^{21} Pa·s for the deep upper mantle, which is higher than 0.3–0.7×10^{21} Pa·s that previous 1-D GIA studies indicate (Steffen *et al.* 2008; Kierulf *et al.* 2014).

Table 2. Overview of the best 10 models and their misfit with respect to the RSL and VLM data calculated separately for the British Isles region (top) and Fennoscandia (bottom). Average viscosity and elastic thickness are computed as described in Section 2.2. 1-D models are highlighted in orange and 3-D models are highlighted in blue.

Rank	Label	Earth model	Rheology parameters	Shallow upper mantle viscosity [10^{21} Pa s]	Deeper upper mantle viscosity [10^{21} Pa s]	Effective elastic lithosphere thickness [km]
						British Isles
1	I6-VM_η=0.3	VM5A profile	$\eta_{upper} = 3 \cdot 10^{20}$	0.30	0.30	70
2	I6-S10W	SMEAN2	10 mm Wet	6.31	0.13	115
3	BI-W7D	WINTERC-G	7 mm Dry	0.56	0.46	97
4	P17-W7D	WINTERC-G	7 mm Dry	0.33	0.58	93
5	I6-VM	VM5A profile	Regular	0.50	0.50	70
6	I6-W8.5D	WINTERC-G	8.5 mm Dry	1.01	0.49	93
7	I6-W10W	WINTERC-G	10 mm Wet	0.10	0.01	70
8	I6-S_β=0.75	SMEAN2	$\beta = 0.75$	3.97	1.16	70
9	BI-VM	VM5A profile	Regular	0.50	0.50	70
10	I6-W10W	WINTERC-G	10 mm Dry	0.77	1.26	147
						Scandinavia
1	I6-W7D	WINTERC-G	7 mm Dry	3.51	1.99	169
2	I6-VM	VM5A	Regular	0.50	0.50	70
3	I6-VM_η=0.3	VM5A	$\eta_{upper} = 3 \cdot 10^{20}$	0.30	0.30	70
4	I6-S_β=0.75	SMEAN2	$\beta = 0.75$	62.6	2.76	135
5	BI-S4/8.5D	SMEAN2	4 mm/8.5 mm Dry	2.51	1.58	189
6	I6-W5.5D	WINTERC-G	5.5 mm Dry	6.31	1.00	131
7	P17-W8.5D	WINTERC-G	8.5 mm Dry	7.41	2.40	147
8	BI-W4D	WINTERC-G	4 mm Dry	12.59	0.50	122
9	P17-W7D	WINTERC-G	7 mm Dry	11.67	2.3	152
10	BI-S_β=0.75	SMEAN2	$\beta = 0.75$	60.6	2.64	137

Legend: BRITICE, ICE-6G, P17. Misfit axis [-] from 0 to 3.

4 DISCUSSION

In this section, we further analyse the fit of the models to RSL and VLM data (Subsections 4.1 and 4.2), the viscosity contrast between Fennoscandia and the British Isles (Subsection 4.3) and the importance of nonlinear rheology (Subsection 4.4).

4.1 High versus low viscosity in Fennoscandia according to RSL data

When examining both the RSL data and VLM data we found improvements using 3-D models when the BRITICE or P17 ice history was used, but no improvement when ICE-6G was used. This suggests that the bias in the ice history towards a viscosity profile is the main reason that no improvement in fit is found for ICE-6G in combination with a 3-D rheology. In Fig. 5(g), we see an example of how low-viscosity models can still result in a decent fit with data in a supposed high-viscosity area according to 3-D models (see Fig. 2). I6-W7D gives a better fit to the data, likely due to the higher viscosity in the region, however the 1-D model with lowered viscosity, I6-VM_η = 3 also improves the fit compared to the reference model. The reference 1-D model results in too much initial deformation and thus a high-initial RSL ($\sim$12 ky B.P.) which worsens the fit. Using the I6-VM_η = 3 model reduces this high-initial RSL due to the shorter relaxation time, resulting in a reduced misfit. The RSL data in the Baltic is too limited temporally to distinguish between a small deflection at 10 ky and subsequent slow relaxation, as predicted by high-viscosity models, or high deflection and subsequent fast relaxation because of low viscosity. However, in combination with the high uplift in Sweden, high-viscosity models produce a better fit in our analysis.

In contrast, we see that in a location at the forebulge such as Samsø the apparent highstand in the data can only be reproduced with the low viscosity present in I6-VM_η = 3. The higher local viscosity in I6-W7D (see Fig. 2) decreases deflection at LGM (see Supplementary Section S.1) and reduces the uplift after that. The increased misfit of that model suggests that the real viscosity there is lower than given by the I6-W7D, consistent with seismic models (French *et al.* 2013; Debayle *et al.* 2016). This is again corroborated by the fact that I6-VM_η = 3 is the best-fitting model in this location. The 3-D models combined with the P17 ice model also performed better here, suggesting that the ice load and its corresponding forebulge location is also of importance.

4.2 Local uplift relation to local and distant viscosity

For the VLM data comparison, a larger misfit is observed for the best 3-D model not based on ICE-6G (BI-S4/8.5D) along the Norwegian west coast (see Fig. 6d), although the viscosity for this 3-D model is similar to that of the 1-D model in this region. This is likely an example of how viscosity variations in adjacent regions can influence the local uplift. This already occurs at the LGM where the deflection pattern is different from that of a 1-D model (Supplementary Section S.1). This demonstrates that the uplift rate pattern of a 3-D model cannot always be replicated with a 1-D model even if it has a local average viscosity equal to that of the 3-D model, stressing the importance of using 3-D rheology.

The reason for the poor performance of the BI-S4/8.5D model when compared to VLM data in the British Isles is hard to pinpoint. It could be that the viscosity of this model is too high in that region. Increasing water content of the British Isles region could be a way to lower viscosity in the region without having to reduce grain size below unfeasible values. However, BI-W7D performs better, which might indicate that the viscosity in western Fennoscandia is too high for BI-S4/8.5D which influences the results in the British

Isles. Finally, it must be noted that in general the combination of BRITICE with VM5a also does not perform as well as ICE-6G models, while in Bradley *et al.* (2023) BRITICE models fit the RSL data better than in this study using a different Earth model. A likely cause is the lower viscosity in the transition zone we used in this study.

4.3 Large viscosity difference between central Fennoscandia and the British Isles

When we consider BRITICE models, which are less tuned to an Earth model, the hybrid model with different grain sizes or water content for different regions (see Section 3.2) did better than other BRITICE models. While 1-D studies in general favour low-upper mantle viscosity, several studies with 1-D models show misfit plots, in which a second region of low misfit exists for high-upper mantle viscosity, matching the high-upper mantle viscosity in the hybrid 3-D earth model (e.g. Davis *et al.* 1999; Schmidt *et al.* 2014; Root *et al.* 2015).

4.4 Nonlinear rheology in Europe

Finally, we investigate the effective viscosity changes in time due to changes in stress (see eq. 4). VLM data is better fitted using Earth models with a high-average viscosity and low-nonlinear properties compared to the models that fit RSL data well. This may be explained in part by the position of the data points. The RSL data is gathered near and just off the coast, where local viscosity tends to be lower in general compared to much of the Fennoscandian GNSS sites which are more inland on top of the craton. However, it might be possible that in addition to this, the RSL data is sensitive to changes in viscosity over geological timescales, while the VLM data is not by nature. The best-fitting models for the British Isles include wet models for which viscosity depends more strongly on stress. This means that the viscosity of the mantle underneath the British Isles might change over time (e.g. Barnhoorn *et al.* 2011). Deglaciation induced stress lowers the effective viscosity so that RSL curves correspond for much of the period with low-viscosity model curves. As the stress dissipates the effective viscosity increases, preventing full relaxation which leads to the low-uplift rates we observe.

In contrast, the only model for Fennoscandia with a strong nonlinear component is the 7 mm model with 50 ppm H_2O content ranked 11th. However, the fit is decent for the same reasons the low-viscosity 1-D model fits some of the data in Fennoscandia, but its maximum uplift is too low as seen in Supplementary Section S.7. The preference for dry rheology agrees with earlier conclusions on a preference for dry rheology for GIA models in van der Wal *et al.* (2013), as well as with Novella *et al.* (2015) who find that diamond samples from cratons contain low amounts of water content. Although Ramirez *et al.* (2024) inferred that there might be high-water content in parts of the Fennoscandian mantle, they also concluded that the rheology underneath Fennoscandia is diffusion dominated, which agrees with the weak nonlinear component we find as a consequence of dry rheology. The best-fitting models as seen in Table 2 have temporal viscosity changes of less than 2×10^{20} Pa·s, considering elements that behave viscously (viscosity $< 10^{23}$ Pa·s) over the model simulation time.

5 CONCLUSION

In this paper, we investigated to what extent a 3-D rheology in a GIA model can improve the fit with relative sea level data and vertical land motion data in Northern Europe. We have run 42 models, of which seven are 1-D and 35 are 3-D models that are combinations of three ice loading histories, two seismic models and two methods to obtain viscosity. 3-D viscosity is used in the upper mantle, split in a shallow (70–180 km) and deep upper mantle (180–400 km depth). The average viscosity values of the shallow and deep upper mantle of these 3-D models ranges between approximately 0.1×10^{21} and 50×10^{21} Pa·s. 3-D models could match but not improve the fit of the VM5a model in combination with ICE-6G (I6-VM) to GNSS and RSL data in Europe which mostly reflects that the I6-VM has been tuned to fit much of the same data used in this study. There are regional differences. For the British Isles that 1-D models perform just as well as the best 3-D models; for Fennoscandia a 3-D model can outperform 1-D models. In particular in the centre and east of Fennoscandia 3-D models consistently fit better than 1-D models.

3-D models result in an improved fit for the ice models which depend less on an *a priori* viscosity model, Patton *et al.* 2017 model (P17) and the BRITICE-CHRONO model (BRITICE). This supports the development of ice sheet histories based on 3-D viscosity as argued by Nordman *et al.* (2015) and Kuchar *et al.* (2019b), and as attempted by Huang *et al.* (2019).The second-best approach would be to use ice sheet histories that are more strongly constrained based on geology or ice sheet physics than by GIA observations through a 1-D GIA model.

Our conclusions are based on 3-D variations in the upper mantle. 3-D viscosity variations in the transition zone influences GIA predictions (Steffen *et al.* 2006; Lau *et al.* 2018) and should be investigated further. As GIA corrections of observations generally do not include 3-D GIA models and lack accurate uncertainty estimates, we suggest that our best-fitting 3-D GIA model can be used as alternative correction for observations of gravity and sea level changes, especially in the Baltic Sea (as in Spada & Galassi 2012) and the Norwegian Atlantic coast and for landscape evolution in Europe (Hijma & Cohen 2011). The model uses a 7 mm dry rheology WINTERC-G upper mantle model and ICE-6G ice history, and its misfit of 1.57 is close to the misfit of the reference 1-D model. The uplift rate is presented in Fig. S10 (Supplementary Material).

Comparing our 3-D model predictions to a limited number of 1-D model predictions showed that the spatial patterns and temporal patterns of the 1-D and best-fitting 3-D models are different in a way that cannot be explained by combining separate 1-D models that have similar average viscosity. This can be seen in Fennoscandia, where 3-D rheology shifts the deflection more westwards because of the high viscosity in the east. This aligns better with the low positive RSL found in the Eastern Baltic Sea and the low-uplift rate in Finland.

GIA studies with 1-D models show little difference in best-fitting upper mantle viscosity between the British Isles and Fennoscandia (Lambeck *et al.* 1998; Steffen *et al.* 2008; Kierulf *et al.* 2014; Simms *et al.* 2022; Bradley *et al.* 2023), even though seismic models show considerable differences in Earth structure. We explored whether the GIA data prefers 3-D models with large or no contrast between the two regions by comparing the median of the best 10 3-D models. The median model viscosity for the British Isles is 0.56×10^{21} and 0.5×10^{21} Pa·s for the shallow and deep upper mantle viscosity, respectively, together with an effective elastic thickness of

70–115 km. In Fennoscandia, the median viscosity is 4.9×10^{21} Pa·s for the shallow upper mantle and 1.3×10^{21} Pa·s for the deeper upper mantle and the region has a thicker elastic lithosphere (122–189 km). This is considerably higher than the global average and findings in previous GIA studies. This shows that a viscosity contrast between regions in Europe is supported by inferences from GIA data.

The performance of all 3-D models enables conclusions about the solid earth parameters. Wet rheology can fit for the British Isles region, although some dry models can also still fit the data in the British Isles to an equal degree if the average viscosity is average or low ($<0.5 \times 10^{21}$ Pa·s). This means that a strong linear component for the mantle underneath the British Isles is a possibility, but not certain. In both cases it would mean that low viscosity has accommodated almost complete relaxation. The Earth structure underneath Fennoscandia is almost certainly dry, as wet rheology leads to underpredicted uplift rate as also shown in van der Wal *et al.* (2013). This agrees with petrological findings that cratons, as found under eastern Fennoscandia, likely have little to no water content (Novella *et al.* 2015). The low-temperature region underneath the North Sea in WINTERC-G had an adverse effect on the fit which means it is either not there or it does not result in a viscosity difference because material parameters offset the effect of the temperature anomaly on viscosity.

ACKNOWLEDGMENTS

SUPPORTING INFORMATION

Supplementary data are available at *GJI* online.

Figure S1. Comparison of LGM deflection. (a) The difference between the deflection at LGM between ICE-6G with SMEAN and a scaling of 0.5 and ICE-6G with VM5a. (b) The difference between the deflection at LGM between the Patton ice history (P17) with WINTERC-G and 7 mm dry rheology and the Patton ice history (P17) with VM5a. Red regions indicate less deflection or a higher forebulge for the 3-D model and the blue regions indicate the reverse. The magenta lines are cross-sections detailed in panels (c)–(e). (c) The cross-section from the Danish coast to Murmansk in panel (a). (d) The cross-section from an offshore location north of Ireland to the Danish coast in panel (b). (e) The cross-section from the Danish coast to Murmansk in panel (b). The red triangles in panels (a)–(e) indicate the point of maximal deflection for the 3-D model, while the blue triangles indicate the point of maximum deflection for the 1-D model.

Figure S2. Mesh for the European region zoomed in on Europe with present day coastline at the first time step (63 ky B.P.) of the model (a), and with the LGM extent of ICE-6G over the present day coastlines (b).

Figure S3. Slices at 110 km (a and c) and 210 km depth (b and d) for both the SMEAN2 model (a and b) and the WINTERC-G model (c and d). In panels (a) and (b), values represent the wave speed anomalies, while values in panels (c) and (d) represent the temperature in Kelvin.

Figure S4. Viscosity at 110 km (a) and 210 km (b) depth for the WINTERC-G model with 4 mm grain size and dry conditions. All values are in 10log of the viscosity in Pa · s.

Figure S5. Viscosity at 110 km (a and c) and 210 km (b and d) depth for the WINTERC-G model with 5.5 mm grain size and dry conditions (a and b) and 8.5 mm grain size (c and d). All values are in 10log of the viscosity in Pa · s.

Figure S6. Viscosity at 110 km (a and c) and 210 km (b and d) depth for the SMEAN2 model with $\beta = 0.75$ (a and b) and $\beta = 0.5$ (c and d). All values are 10log of the viscosity in Pa · s.

Figure S7. Selected ice history input used for this study. The top row (a, b and c) shows the ice sheet thickness in Europe at 26 ky B.P. which is near each of their glacial maxima, while the bottom row shows the ice sheet thickness for each history just before the oldest data points (12 ky B.P.). Panels (a) and (d) show BRITICE, (b) and (e) show ICE-6G and (c) and (f) show the Patton model at the same points in time.

Figure S8. Difference in uplift rate when the transition zone viscosity is increased by one order of magnitude for the reference model (a) and a version of the reference model where the upper mantle viscosity has also increased by one order of magnitude (b).

Figure S9. Difference in RSL when the transition zone viscosity is increased by one order of magnitude for the reference model (a and c) and a version of the reference model where the upper mantle viscosity has also increased by one order of magnitude (b and d). Panels (a) and (b) represent RSL changes at 10.5 ky B.P. Panels (c) and (d) represent RSL changes at 7 ky B.P.

Figure S10. Present-day uplift in Europe for model I6-W7D.

Figure S11. RSL in Europe for model I6-W7D for the period between 12 and 4 ky B.P for different epochs: (a) 12 ky B.P., (b) 10.5 ky B.P., (c) 9 ky B.P., (d) 7 ky B.P., (e) 6 ky B.P. and (f) 4 ky B.P.

Table S1. Overview of models with combined misfit with respect to the RSL and VLM data for with a normalization according to eq. (E1). The Earth model structure is in the middle column, with additional details that are used to create each model in the final column. The bars represent the total misfit, with the colours detailing the ice model used.

Table S2. Top five best-fitting models and corresponding misfit with respect to the RSL and VLM data when the influence range for weighing each data point is altered. (a) Halved influence range for weighting data points combined. (b) Doubled influence range for weighting data points. The Earth model structure is in the middle column, with additional details that are used to create each model in the final column. The bars represent the total misfit, with the colours detailing the ice model used.

Table S3. Overview of all run models and corresponding misfit with respect to the RSL and VLM data combined with an altered area for which data is considered. (a) The combined misfit when more data is considered in the analysis. (b) The combined misfit results when less data is considered in the analysis. The Earth model structure is in the middle column, with additional details that are used to create each model in the final column. The bars represent the total misfit, with the colours detailing the ice model used.

Table S4. Overview of all run models. First column: basic earth model label. Second column: rheology parameters to determine the

exact Earth structure. Finally, these Earth models are run with one of three ice sheet reconstructions (third column).

Table S5. Misfit of the 15 models with the lowest combined misfit ordered by misfit value. Model labels start with the ice model, with I6 denoting ICE-6G, BI denoting BRITICE and P17 denoting the model from Patton et al. (2017). The label for the Earth model is denoted after the dash; Earth labels starting with an S are based on SMEAN2 and labels with a W are based on WINTERC-5.2 and the rest of the label denotes the parameters used. The first number is the grain size used in mm and the letter after indicating the water content, dry (D), damp (Da) or wet (W). Alternatively, a β denotes scaled seismic anomalies and the used scaling factor. Earth models with VM indicate a VM5a type 1-D model, with the default viscosity being 5×10^{20} Pa s unless stated otherwise. A bold font is used in the maximum uplift column to denote models that are disqualified for not reaching the measured maximum uplift at a measurement point in central Fennoscandia (8.0 mm yr^{-1}).

Please note: Oxford University Press is not responsible for the content or functionality of any supporting materials supplied by the authors. Any queries (other than missing material) should be directed to the corresponding author for the paper.

DATA AVAILABILITY

Output of the GIA models at the locations and times of the data is available at: http://doi.org/10.4121/d1010e1d-8503-43fa-9df8-cce304b2af47. The ice sheet histories are available from authors of the cited publications. The SMEAN2 seismic model is available at: https://www-udc.ig.utexas.edu/external/becker/tdata.html. WINTERC-G is available at: https://zenodo.org/records/5730195.

REFERENCES

Altamimi, Z., Collilieux, X. & Métivier, L. 2011. ITRF2008: an improved solution of the international terrestrial reference frame, *J. Geod.,* **85,** 457–473.

Amante, C. & Eakins, B.W. 2009. ETOPO1 1 Arc-Minute Global Relief Model: Procedures, Data Sources and Analysis. *NOAA Technical Memorandum NESDIS NGDC-24,* National Geophysical Data Center, NOAA.

Barletta, V.R. *et al.* 2018. Observed rapid bedrock uplift in Amundsen Sea embayment promotes ice-sheet stability, *Science,* **360**(6395), 1335–1339.

Barnhoorn, A., van der Wal, W. & Drury, M.R. 2011. Upper mantle viscosity and lithospheric thickness under Iceland, *J. Geodyn.,* **52**(3–4), 260–270.

Blank, B., Barletta, V., Hu, H., Pappa, F. & van der Wal, W. 2021. Effect of lateral and stress-dependent viscosity variations on GIA induced uplift rates in the Amundsen Sea embayment, *Geochem. Geophys. Geosyst.,* **22**(9), e2021GC009807.

Bradley, S.L., Ely, J.C., Clark, C.D., Edwards, R.J. & Shennan, I. 2023. Reconstruction of the palaeo-sea level of Britain and Ireland arising from empirical constraints on ice extent: implications for regional sea level forecasts and North American ice sheet volume, *J. Quat. Sci.,* **38**(6), 791–805.

Bradley, S.L., Milne, G.A., Shennan, I. & Edwards, R. 2011. An improved glacial isostatic adjustment model for the British Isles, *J. Quat. Sci.,* **26**(5), 541–552.

Celli, N.L., Lebedev, S., Schaeffer, A.J. & Gaina, C. 2021. The tilted Iceland Plume and its effect on the North Atlantic evolution and magmatism, *Earth Planet. Sci. Lett.,* **569,** 117 048.

Clark, C.D. *et al.* 2018. BRITICE Glacial Map, version 2: a map and GIS database of glacial landforms of the last British–Irish Ice Sheet, *Boreas,* **47,** 11–27. 10.1111/bor.12273.

Creel, R.C., Austermann, J., Khan, N.S., D'Andrea, W.J., Balascio, N., Dyer, B., Ashe, E. & Menke, W. 2022. Postglacial relative sea level change in Norway, *Quat. Sci. Rev.,* **282,** 107 422.

Davis, J.L., Mitrovica, J.X., Scherneck, H. & Fan, H. 1999. Investigations of Fennoscandian glacial isostatic adjustment using modern sea level records, *J. Geophys. Res.: Solid Earth,* **104**(B2), 2733–2747.

Debayle, E., Dubuffet, F. & Durand, S. 2016. An automatically updated S-wave model of the upper mantle and the depth extent of azimuthal anisotropy, *Geophys. Res. Lett.,* **43**(2), 674–682.

Fichtner, A. *et al.* 2018. The collaborative seismic Earth model: generation 1, *Geophys. Res. Lett.,* **45**(9), 4007–4016.

Fjeldskaar, W., 1994. The amplitude and decay of the glacial forebulge in Fennoscandia, *Norsk Geologisk Tidsskrift,* **74,** 1 2–8.

Fjeldskaar, W., 1997. Flexural rigidity of Fennoscandia inferred from the postglacial uplift, *Tectonics,* **16,** 4 596–608.

Fleming, K., Martinec, Z. & Wolf, D.& 2002. A reinterpretation of the Fennoscandian relaxation-time spectrum for a viscoelastic lithosphere, *Gravity Geoid 2002, 3rd meeting of the International Gravity and Geoid Commission,* Ziti Publishing, pp. 432–438.

French, S., Lekic, V. & Romanowicz, B. 2013. Waveform tomography reveals channeled flow at the base of the oceanic asthenosphere, *Science,* **342**(6155), 227–230.

Fullea, J., Lebedev, S., Martinec, Z. & Celli, N.L. 2021. WINTERC-G: mapping the upper mantle thermochemical heterogeneity from coupled geophysical–petrological inversion of seismic waveforms, heat flow, surface elevation and gravity satellite data, *Geophys. J. Int.,* **226**(1), 146–191.

García-Artola, A., Stéphan, P., Cearreta, A., Kopp, R.E., Khan, N.S. & Horton, B.P. 2018. Holocene sea-level database from the Atlantic coast of Europe, *Quat. Sci. Rev.,* **196,** 177–192.

Gowan, E.J., Tregoning, P., Purcell, A., Lea, J., Fransner, O.J., Noormets, R. & Dowdeswell, J.A. 2016. ICESHEET 1.0: a program to produce paleo-ice sheet reconstructions with minimal assumptions, *Geosci. Model. Dev.,* **9**(5), 1673–1682.

Hijma, M.P. & Cohen, K.M. 2011. Holocene transgression of the Rhine river mouth area, the Netherlands/Southern North Sea: palaeogeography and sequence stratigraphy, *Sedimentology,* **58**(6), 1453–1485.

Hijma, M.P. & Cohen, K.M. 2019. Holocene sea-level database for the Rhine-Meuse Delta, the Netherlands: implications for the pre-8.2 ka sea-level jump, *Quat. Sci. Rev.,* **214,** 68–86.

Hirth, G. & Kohlstedt, D. 2004. Rheology of the upper mantle and the mantle wedge: a view from the experimentalists, *Geophysical Monograph-American Geophysical Union,* Vol. **138,** Blackwell Publishing Ltd, pp. 83–106.

Huang, P., Wu, P. & Steffen, H., 2019. In search of an ice history that is consistent with composite rheology in Glacial Isostatic Adjustment modelling, *Earth and Planetary Science Letters,* **517,** 26–37.

Hughes, A.L.C., Gyllencreutz, R., Lohne, Ø.S., Mangerud, J. & Svendsen, J.I. 2016. The last Eurasian ice sheets–a chronological database and time-slice reconstruction, DATED-1, *Boreas,* **45**(1), 1–45.

Ivins, E.R. & Sammis, C.G. 1995. On lateral viscosity contrast in the mantle and the rheology of low-frequency geodynamics, *Geophys. J. Int.,* **123**(2), 305–322.

Jackson, M.G., Konter, J.G. & Becker, T.W. 2017. Primordial helium entrained by the hottest mantle plumes, *Nature,* **542**(7641), 340–343.

Karato, S. 2008. , *Deformation of Earth Materials. An Introduction to the Rheology of Solid Earth,* Vol. **463,** Cambridge University Press, Cambridge.

Kaufmann, G. & Lambeck, K. 2000. Mantle dynamics, postglacial rebound and the radial viscosity profile, *Phys. Earth planet. Inter.,* **121**(3), 301–324.

Kendall, R.A., Mitrovica, J.X. & Milne, G.A. 2005. On post-glacial sea level–II. Numerical formulation and comparative results on spherically symmetric models, *Geophys. J. Int.,* **161**(3), 679–706.

Kierulf, H.P., Steffen, H., Barletta, V.R., Lidberg, M., Johansson, J., Kristiansen, O. & Tarasov, L. 2021. A GNSS velocity field for geophysical applications in Fennoscandia, *J. Geodyn.,* **146,** 101 845.

Kierulf, H.P., Steffen, H., Simpson, M.J.R., Lidberg, M., Wu, P. & Wang, H. 2014. A GPS velocity field for Fennoscandia and a consistent comparison to glacial isostatic adjustment models, *J. Geophys. Res.: Solid Earth,* **119**(8), 6613–6629.

Klemann, V. & Wolf, D. 2005. The eustatic reduction of shoreline dia-
grams: implications for the inference of relaxation-rate spectra and the
viscosity stratification below Fennoscandia, *Geophys. J. Int.,* **162**(1),
249–256.

Kuchar, J., Milne, G. & Latychev, K. 2019a. The importance of lateral Earth
structure for North American glacial isostatic adjustment, *Earth Planet.
Sci. Lett.,* **512**, 236–245.

Kuchar, J., Milne, G., Hill, ., Tarasov, L. & & Nordman, M., 2019b. An
investigation into the sensitivity of postglacial decay times to uncertainty
in the adopted ice history, *Geophysical Journal International,* ().

Kuchar, J., Milne, G., Hubbard, A., Patton, H., Bradley, S., Shennan, I. &
Edwards, R. 2012. Evaluation of a numerical model of the British–Irish
ice sheet using relative sea-level data: implications for the interpretation
of trimline observations, *J. Quat. Sci.,* **27**(6), 597–605.

Lambeck, K. 1993. Glacial rebound of the British Isles—I. Preliminary
model results, *Geophys. J. Int.,* **115**(3), 941–959.

Lambeck, K., Johnston, P., Smither, C. & Nakada, M. 1996. Glacial rebound
of the British Isles—III. Constraints on mantle viscosity, *Geophys. J. Int.,*
125(2), 340–354.

Lambeck, K., Smither, C. & Johnston, P. 1998. Sea-level change, glacial re-
bound and mantle viscosity for northern Europe, *Geophys. J. Int.,* **134**(1),
102–144.

Lau, H. C. P., Austermann, J., Mitrovica, J. X., Crawford, O., Al-Attar,
D. & Latychev, K., 2018. Inferences of Mantle Viscosity Based on Ice
Age Data Sets: The Bias in Radial Viscosity Profiles Due to the Neglect
of Laterally Heterogeneous Viscosity Structure, *Journal of Geophysical
Research: Solid Earth,* **123** (9), 7237.

Li, T. & Wu, P. 2019. Laterally heterogeneous lithosphere, asthenosphere
and sub-lithospheric properties under Laurentia and Fennoscandia from
Glacial Isostatic Adjustment, *Geophys. J. Int.,* **216**(3), 1633–1647.

Lidberg, M., Johansson, J., Scherneck, H.-G. & Milne, G. 2010. Recent
results based on continuous GPS observations of the GIA process in
Fennoscandia from BIFROST, *J. Geodyn.,* **50**, 8–18.

Mäkinen, J. et al. 2006. Regional Adjustment of Precise Levellings around
the Baltic, *Mitteilungen des Bundesamtes fürKartographie und Geodäsie,*
35, EUREF Publication No. 15.

Marotta, A.M. & Sabadini, R. 2002. Tectonic versus glacial isostatic defor-
mation in Europe, *Geophys. Res. Lett.,* **29**(10), 73–71-73-74.

Milne, G.A., Davis, J.L., Mitrovica, J.X., Scherneck, H.-G., Johansson,
J.M., Vermeer, M. & Koivula, H. 2001. Space-geodetic constraints
on glacial isostatic adjustment in Fennoscandia, *Science,* **291**(5512),
2381–2385.

Milne, G.A., Mitrovica, J.X., Scherneck, H.-G., Davis, J.L., Johansson, J.M.,
Koivula, H. & Vermeer, M. 2004. Continuous GPS measurements of
postglacial adjustment in Fennoscandia: 2. Modeling results, *J. Geophys.
Res.: Solid Earth,* **109**(B2),.

Nordman, M., Milne, G. & Tarasov, L. 2015. Reappraisal of the Ångerman
River decay time estimate and its application to determine uncertainty in
Earth viscosity structure, *Geophys. J. Int.,* **201**(2), 811–822.

Novella, D., Bolfan-Casanova, N., Nestola, F. & Harris, J.W. 2015. H₂O
in olivine and garnet inclusions still trapped in diamonds from the Siberian
craton: implications for the water content of cratonic lithosphere peri-
dotites, In *Lithos,* Vol. **230**, pp. 180–183, Elsevier B.V.

Patton, H. et al. 2017. Deglaciation of the Eurasian ice sheet complex, *Quat.
Sci. Rev.,* **169**, 148–172.

Patton, H., Hubbard, A., Andreassen, K., Winsborrow, M. & Stroeven,
A.P. 2016. The build-up, configuration, and dynamical sensitivity of the
Eurasian ice-sheet complex to late weichselian climatic and oceanic forc-
ing, *Quat. Sci. Rev.,* **153**, 97–121.

Peeters, J., Busschers, F.S. & Stouthamer, E. 2015. Fluvial evolution of the
Rhine during the last interglacial-glacial cycle in the southern North Sea
basin: a review and look forward, *Quat. Int.,* **357**, 176–188.

Peltier, W.R. 2004. Global glacial isostasy and the surface of the ice-age
Earth: the ICE-5 G (VM2) model and GRACE, *Annu. Rev. Earth Planet.
Sci.,* **32**(1), 111–149.

Peltier, W.R., Argus, D.F. & Drummond, R. 2015. Space geodesy constrains
ice age terminal deglaciation: the global ICE-6G_C (VM5a) model, *J.
Geophys. Res.: Solid Earth,* **120**(1), 450–487.

Powell, E., Latychev, K., Gomez, N. & Mitrovica, J.X. 2022. The robustness
of geodetically derived 1-D antarctic viscosity models in the presence
of complex 3-D viscoelastic Earth structure, *Geophys. J. Int.,* **231**(1),
118–128.

Ramirez, F.D.C., Selway, K., Conrad, C.P., Maupin, V. & Smirnov, M. 2024.
Lateral and radial viscosity structure beneath Fennoscandia inferred from
seismic and magnetotelluric observations, *Phys. Earth planet. Inter.,* **351**,
107 178.

Richter, A., Groh, A. & Dietrich, R. 2012. Geodetic observation of sea-level
change and crustal deformation in the Baltic Sea region, *Phys. Chem.
Earth,* **53–54**, 43–53.

Roberts, M., Scourse, J., Bennell, J., Huws, D., Jago, C. & Long, B. 2011.
Late devensian and holocene relative sea-level change in North Wales,
UK, *J. Quat. Sci.,* **26**, 141–155.

Root, B.C., van der Wal, W., Novák, P., Ebbing, J. & Vermeersen, L.L.A.
2015. Glacial isostatic adjustment in the static gravity field of Fennoscan-
dia, *J. Geophys. Res.: Solid Earth,* **120**(1), 503–518.

Rosentau, A. et al. 2021. A Holocene relative sea-level database for the
Baltic Sea, *Quat. Sci. Rev.,* **266**, doi: 10.1016/j.quascirev.2021.107071.

Rosentau, A., Harff, J., Oja, T. & Meyer, M. 2012. Postglacial rebound and
relative sea level changes in the Baltic Sea since the Litorina transgression,
Baltica, **25**(2), pp. 113–120, doi: 10.5200/baltica.2012.25.11.

Rovira-Navarro, M., van der Wal, W., Barletta, V.R., Root, B.C. & Sandberg
Sørensen, L. 2020. GRACE constraints on Earth rheology of the Barents
Sea and Fennoscandia, *Solid Earth,* **11**(2), 379–395.

Rushby, G.T., Richards, G.T., Gehrels, W.R., Anderson, W.P., Bateman, M.D.
& Blake, W.H. 2019. Testing the mid-holocene relative sea-level highstand
hypothesis in North Wales, UK, *The Holocene,* **29**(9), 1491–1502.

Schaeffer, A.J. & Lebedev, S. 2013. Global shear speed structure of the
upper mantle and transition zone, *Geophys. J. Int.,* **194**(1), 417–449.

Schmidt, P., Lund, B., Näslund, J.-O. & Fastook, J. 2014. Comparing a
thermo-mechanical Weichselian Ice Sheet reconstruction to reconstruc-
tions based on the sea level equation: aspects of ice configurations and
glacial isostatic adjustment, *Solid Earth,* **5**(1), 371–388.

Schumacher, M., King, M.A., Rougier, J., Sha, Z., Khan, S.A. & Bamber,
J.L. 2018. A new global GPS data set for testing and improving modelled
GIA uplift rates, *Geophys. J. Int.,* **214**(3), 2164–2176.

Shapiro, N.M. & Ritzwoller, M.H. 2002. Monte-Carlo inversion for a global
shear-velocity model of the crust and upper mantle, *Geophys. J. Int.,*
151(1), 88–105.

Shennan, I., Bradley, S.L. & Edwards, R. 2018. Relative sea-level changes
and crustal movements in Britain and Ireland since the Last Glacial max-
imum, *Quat. Sci. Rev.,* **188**, 143–159.

Simms, A.R. et al. 2022. Investigating the roles of relative sea-level change
and glacio-isostatic adjustment on the retreat of a marine based ice stream
in NW Scotland, *Quat. Sci. Rev.,* **277**, 107 366.

Simon, K.M. & Riva, R.E.M. 2020. Uncertainty estimation in regional
models of long-term GIA uplift and sea level change: an overview, *J.
Geophys. Res.: Solid Earth,* **125**(8), e2019JB018983.

Simon, K.M., Riva, R.E.M. & Vermeersen, L.L.A. 2021. Constraint of
glacial isostatic adjustment in the North Sea with geological relative
sea level and GNSS vertical land motion data, *Geophys. J. Int.,* **227**(2),
1168–1180.

Spada, G. & Galassi, G. 2012. New estimates of secular sea level rise from
tide gauge data and GIA modelling, *Geophys. J. Int.,* **191**(3), no–no.

Steffen, H. & Kaufmann, G. 2005. Glacial isostatic adjustment of Scandi-
navia and northwestern Europe and the radial viscosity structure of the
Earth's mantle, *Geophys. J. Int.,* **163**(2), 801–812.

Steffen, H., Denker, H. & Müller, J. 2008. Glacial isostatic adjustment in
Fennoscandia from GRACE data and comparison with geodynamical
models, *J. Geodyn.,* **46**(3), 155–164.

Steffen, H., Kaufmann, G. & Lampe, R. 2014. Lithosphere and upper-
mantle structure of the southern Baltic Sea estimated from modelling
relative sea-level data with glacial isostatic adjustment, *Solid Earth,* **5**(1),
447–459.

Steffen, H., Kaufmann, G. & Wu, P. 2006. Three-dimensional finite-element
modeling of the glacial isostatic adjustment in Fennoscandia, *Earth
planet. Sci. Lett.,* **250**(1–2), 358–375.

Steffen, H., Wu, P. & Wang, H. 2010. Determination of the Earth's structure in Fennoscandia from GRACE and implications for the optimal post-processing of GRACE data, *Geophys. J. Int.,* **182**(3), 1295–1310.

Tanaka, Y., Klemann, V., Fleming, K. & Martinec, Z. 2009. Spectral finite element approach to postseismic deformation in a viscoelastic self-gravitating spherical Earth, *Geophys. J. Int.,* **176**(3), 715–739.

Turcotte, D.L. & Schubert, G. 2002. *Geodynamics*. Cambridge University Press.

van der Wal, W., Wu, P., Wang, H. & Sideris, M.G. 2010. Sea levels and uplift rate from composite rheology in glacial isostatic adjustment modeling, *J. Geodyn.,* **50**(1), 38–48.

vand er Wal, W., Barnhoorn, A., Stocchi, P., Gradmann, S., Wu, P., Drury, M. & Vermeersen, B. 2013. Glacial isostatic adjustment model with composite 3-D earth rheology for Fennoscandia, *Geophys. J. Int.,* **194**(1), 61–77.

Vestøl, O., Ågren, J., Steffen, H., Kierulf, H. & Tarasov, L. 2019. NKG2016LU: a new land uplift model for Fennoscandia and the Baltic Region, *J. Geod.,* **93**(9), 1759–1779 .

Wahl, T., Jensen, J. & Frank, T. 2010. On analysing sea level rise in the German Bight since 1844, *Nat. Hazards Earth Syst. Sci.,* **10**(2), 171–179.

Wieczerkowski, K., Mitrovica, J.X. & Wolf, D. 1999. A revised relaxation-time spectrum for Fennoscandia, *Geophys. J. Int.,* **139**(1), 69–86.

Wu, P., 2004. Using commercial finite element packages for the study of earth deformations, sea levels and the state of stress, *Geophys. J. Int.,* **158**, 401–408.

Wu, P. 2002. Mode coupling in a viscoelastic self-gravitating spherical earth induced by axisymmetric loads and lateral viscosity variations, *Earth Planet. Sci. Lett.,* **202**(1), 49–60.

Wu, P., Wang, H. & Steffen, H. 2013. The role of thermal effect on mantle seismic anomalies under Laurentia and Fennoscandia from observations of Glacial Isostatic Adjustment, *Geophys. J. Int.,* **192**(1), 7–17.

Yousefi, M., Milne, G.A. & Latychev, K. 2021. Glacial isostatic adjustment of the Pacific Coast of North America: the influence of lateral Earth structure, *Geophys. J. Int.,* **226**(1), 91–113.

Zhao, S., Lambeck, K. & Lidberg, M. 2012. Lithosphere thickness and mantle viscosity inverted from GPS-derived deformation rates in Fennoscandia, *Geophys. J. Int.,* **190**(1), 278–292.